TITLE:

Crystallographic and superconducting properties of the fully gapped noncentrosymmetric 5d-electron superconductors CaMSi_{3} (M= Ir, Pt)

AUTHOR(S):

Eguchi, G.; Peets, D.; Kriener, M.; Maeno, Y.; Nishibori, E.; Kumazawa, Y.; Banno, K.; Maki, S.; Sawa, H.

CITATION:

Eguchi, G. ...[et al]. Crystallographic and superconducting properties of the fully gapped noncentrosymmetric 5d-electron superconductors CaMSi_{3} (M= Ir, Pt). Physical Review B 2011, 83(2): 024512.

ISSUE DATE:

2011-01

URL:

http://hdl.handle.net/2433/138098

RIGHT:

© 2011 by American Physical Society.

京都大学学術情報リポジトリ
KURENAI 紅
Kyoto University Research Information Repository

京都大学 KYOTO UNIVERSITY
A Self-archived copy in
Kyoto University Research Information Repository
https://repository.kulib.kyoto-u.ac.jp
京都大学学術情報リポジトリ KURENAI 紅 Kyoto University Research Information Repository

PHYSICAL REVIEW B **83**, 024512 (2011)

Crystallographic and superconducting properties of the fully gapped noncentrosymmetric 5*d*-electron superconductors CaMSi$_3$ (M = Ir, Pt)

G. Eguchi,* D. C. Peets, M. Kriener, and Y. Maeno
Department of Physics, Graduate School of Science, Kyoto University, Kyoto 606-8502, Japan

E. Nishibori, Y. Kumazawa, K. Banno, S. Maki, and H. Sawa
Department of Applied Physics, Graduate School of Engineering, Nagoya University, Nagoya 464-8603, Japan
(Received 21 June 2010; revised manuscript received 1 December 2010; published 31 January 2011)

We report crystallographic, specific heat, transport, and magnetic properties of the recently discovered noncentrosymmetric 5*d*-electron superconductors CaIrSi$_3$ (T_c = 3.6 K) and CaPtSi$_3$ (T_c = 2.3 K). The specific heat suggests that these superconductors are fully gapped. The upper critical fields are less than 1 T, consistent with limitation by conventional orbital depairing. High, non-Pauli-limited $\mu_0 H_{c2}$ values, often taken as a key signature of novel noncentrosymmetric physics, are not observed in these materials because the high carrier masses required to suppress orbital depairing and reveal the violated Pauli limit are not present.

DOI: 10.1103/PhysRevB.83.024512 PACS number(s): 74.25.Dw, 61.66.Fn, 74.20.Rp

I. INTRODUCTION

There has been a great deal of interest in noncentrosymmetric superconductors initiated by the discovery of highly unconventional behavior in CePt$_3$Si.[1] The overwhelming majority of superconductors studied to date have crystal structures exhibiting inversion symmetry. If an inversion element is present, inversion about the origin in momentum space can at most change the sign of the superconducting pairing function, which can thus be classified by its parity, and the spin state of the pairs must be either symmetric or antisymmetric (triplet or singlet) on exchange of the component fermions. In structures lacking an inversion element, however, there is no such constraint, parity is not a meaningful label, and pairing states cannot be classified as singlet or triplet. In such a material, spin-orbit terms can split the underlying band structure, and thus the Fermi surface, by spin orientation. Where the splitting is large compared to the superconducting gap, pairing is expected to occur only within each Fermi surface sheet, and since there is only one allowed spin orientation at any given point on each sheet, the pairing state will be a mixture of what would normally be regarded as singlet and triplet components. A wide variety of exotic superconducting properties have been predicted in noncentrosymmetric superconductors,[2–5] but many have not yet been observed.

A number of other noncentrosymmetric superconductors have since been reported and are being actively studied, including UIr,[6] CeRhSi$_3$,[7] Ir$_2$Ga$_9$,[8] and B-doped SiC.[9] Exotic properties, however, have so far mostly been observed in materials containing cerium, and cerium compounds commonly exhibit unusual magnetism; the magnetism and superconductivity are thought to originate from the same itinerant 4*f* electrons. Disentangling the not-fully-understood, novel noncentrosymmetric physics from the complications introduced by strongly correlated *f* electrons of heavy-fermion compounds remains a key challenge, and will require the study of nonmagnetic, *f*-electron-free noncentrosymmetric superconductors. Thus far, the only *d*-electron systems in which unconventional behavior has been reported that might arise from the lack of inversion symmetry are Li$_2$Pt$_3$B[10,11] and LaNiC$_2$.[12]

Recently, nine new noncentrosymmetric superconductors were reported with the same crystal structure as CeRhSi$_3$ (space group $I4mm$),[13,14] with chemical formulas AMSi$_3$ (A = Ca, Sr, Ba; M = Co, Rh, Ir, Ni, Pd, Pt). All are thought to be nonmagnetic, and none contain active *f* electrons. These materials are uniquely valuable because they can be readily compared to Ce-containing superconductors with an identical crystal structure. Unlike their Ce-based analogs, in which superconductivity only emerges at high pressures once antiferromagnetism has been suppressed,[15–17] the newly discovered materials superconduct at ambient pressure. This is suggestive of a magnetic pairing mechanism for the Ce-based materials and a more conventional phonon mechanism for the new materials.

The new *f*-electron-free 1-1-3 silicides have the potential to be the subject of intense research. A key first step is basic characterization of the superconducting state. To this end, we prepared polycrystalline samples of the CaMSi$_3$ materials (M = Ir, Pt) that would be expected to have the strongest spin-orbit interactions, and investigated their structure, specific heat, resistivity, and magnetic properties.

II. SAMPLE PREPARATION AND CHARACTERIZATION

Polycrystalline samples were prepared from CaSi (99.9%, Furuuchi Chemical, 1–3 mm granule), Ir (99.99%, Furuuchi Chemical, powder), Pt (99.98%, Nilaco, powder), and Si (99.999%, Furuuchi Chemical, powder) by arc melting. The raw materials were ground under nitrogen to avoid oxidation, then pressed into a pellet, and melted under argon. Samples synthesized starting from the nominal composition of Ca:Ir:Si = 1:1:3 produced the new material CaIr$_3$Si$_7$, discussed in the appendix. To compensate for loss of volatile calcium silicides, molar ratios of Ca:Ir:Si = 3:1:4.7 and Ca:Pt:Si = 3:1:5 were used. Powder x-ray diffraction (XRD) was performed with a commercial x-ray diffractometer (MAC Science, M03XHT^{22}) using CuKα radiation (wavelength: 1.54056 Å), and surface analyses using a commercial scanning electron microscope (SEM, Keyence VE-9800S) and energy-dispersive x-ray spectrometer (EDX, EDAX VE7800), all at room temperature. The results are presented in Fig. 1. Both the CaIrSi$_3$ and CaPtSi$_3$ samples exhibited additional XRD peaks from impurity phases, but were of high enough quality that their superconducting properties could be investigated. The inset of

 ©2011 American Physical Society

京都大学 KYOTO UNIVERSITY
A Self-archived copy in
Kyoto University Research Information Repository
https://repository.kulib.kyoto-u.ac.jp
京都大学学術情報リポジトリ KURENAI 紅 Kyoto University Research Information Repository

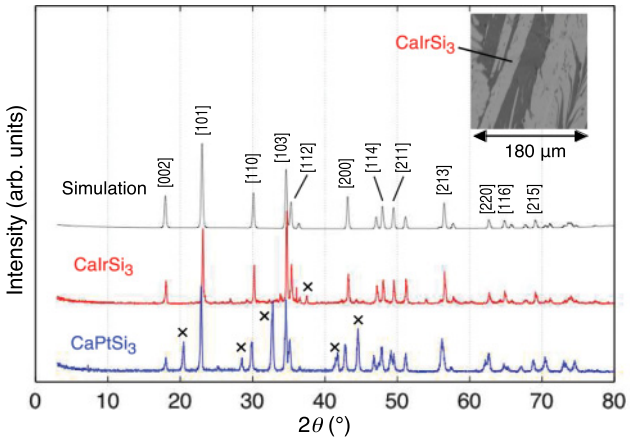

FIG. 1. (Color online) Powder x-ray-diffraction results for $CaIrSi_3$ and $CaPtSi_3$. The crosses indicate impurity peaks. The inset displays a scanning electron micrograph of $CaIrSi_3$. The sample contained an impurity phase. The EDX result reveals the bright area to be $CaIrSi_3$ and the dark area to have the approximate cation ratio of Ca:Ir:Si = 1:0:2.28.

Fig. 1 displays a SEM image. EDX composition mapping identified two distinct phases in the $CaIrSi_3$ sample, with approximate cation ratios Ca:Ir:Si = 1:1.03:2.95, consistent with $CaIrSi_3$, and Ca:Ir:Si = 1:0:2.28. The Ir-free phase did not appear in XRD, suggesting it to be solidified melt without a well-defined crystal structure.

Single-phase $CaIrSi_3$ grains of size ~200 μm were isolated using dilute hydrochloric acid, then crushed. Homogeneous micron-sized grains were selected using an ethanol suspension, then sealed in a Lindemann glass capillary of internal diameter 0.2 mm. High-resolution synchrotron XRD measurements were performed in transmission mode at the SPring-8 BL02B2 beam line using N_2 gas-flow temperature control and a large Debye-Scherrer camera with an imaging plate detector[18] which was set up to collect data from 0.010 to 78.68° in 2θ, with a resolution of 0.010°. Data were collected at a series of temperatures from 90 to 300 K with exposure times of 5 minutes, and a higher-statistics dataset with a 60-minute exposure time was taken on a different sample at 100 K for structure refinement. The highest peak in the latter dataset had approximately 1,100,000 counts. An incident x-ray wavelength of 0.357 47(1) Å was used, calibrated with a CeO_2 standard.

No technique was found that would result in single-phase $CaPtSi_3$ grains, but aqua regia dissolved most impurities, and it was also possible to isolate $CaPtSi_3$-free grains of the remaining impurity phases. Spectra with and without $CaPtSi_3$ were collected as for $CaIrSi_3$, using a wavelength of 0.351 190(12) Å, but without a high-statistics dataset. By comparing the $CaPtSi_3$ and impurity-phase spectra, reflections associated with impurity phases could be deleted, allowing structure refinements for $CaPtSi_3$ as shown in Fig. 1. The previously mentioned limitations require that the $CaPtSi_3$ XRD results be treated with caution, but they should provide a useful starting point.

Both compounds' lattice parameters increase monotonically with temperature by less than 0.4% over the temperature range probed, as displayed in Fig. 2 for $CaIrSi_3$. In this

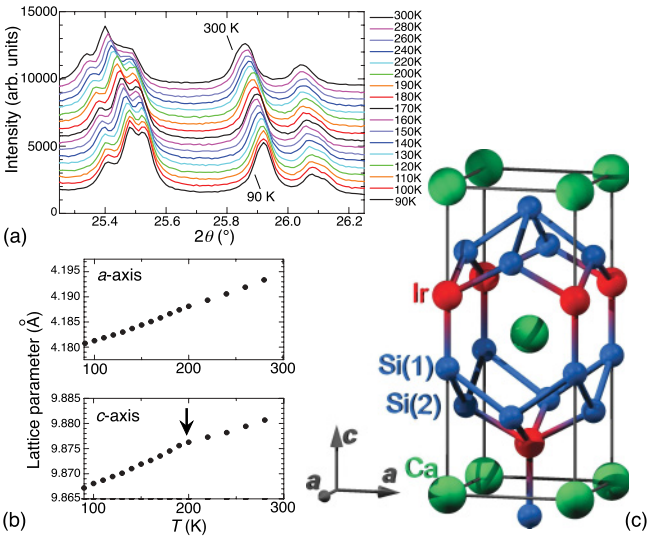

FIG. 2. (Color online) X-ray-diffraction results on $CaIrSi_3$: (a) Temperature dependence of several powder XRD peaks of $CaIrSi_3$ from 90 K (bottom) to 300 K (top) with an incident x-ray wavelength of 0.357 47(1) Å. (b) Temperature dependence of both lattice parameters. A slight slope change is visible for the c axis at 200 K. (c) Noncentrosymmetric crystal structure of $CaIrSi_3$ as determined by powder x-ray diffraction.

compound only, a small slope change in the c-axis lattice parameter can be seen at 200 K, and the c-axis position of the Si(2) (Ir–Si layer) site appears to fall by about 0.005 Å above this temperature, making the Ir–Si layer slightly flatter. The above changes were reflected in the interatomic distances.

Figure 3 and Table I report the results of a Rietveld structure refinement performed on the higher-statistics $CaIrSi_3$ data using the program Synchrotron-Powder,[19] using 1086 reflections from 2.500° to 75.000°. The reliability factors based on the weighted profile, R_{wp}, and on the Bragg intensities, R_I, were 4.30% and 1.98%, respectively. Refinements of the temperature-dependent $CaPtSi_3$ data typically produced reliability factors R_{wp} and R_I of 4.8%–5.1% and 7.0%–8.5%,

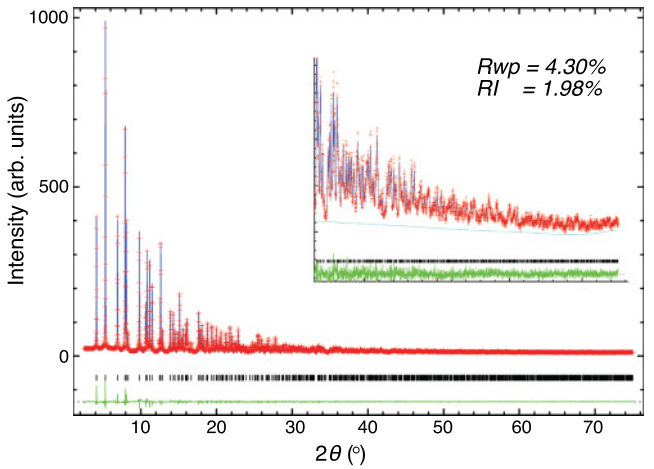

FIG. 3. (Color online) The Rietveld structure refinement of $CaIrSi_3$ performed on the higher-statistics synchrotron x-ray data at 100 K.

京都大学 KYOTO UNIVERSITY
A Self-archived copy in
Kyoto University Research Information Repository
https://repository.kulib.kyoto-u.ac.jp
京都大学学術情報リポジトリ KURENAI 紅 Kyoto University Research Information Repository

TABLE I. The lattice parameters, fractional atomic coordinates, and interatomic distances of $CaIrSi_3$ at 100 K. U(iso) is the isotropic thermal displacement parameter.

Refinement				
Space group	Tetragonal, $I4mm$ (No. 107)			
Z/calculated density	2/6.085 Mg/m^3			
Absorption coefficient	5.732 mm^{-1}			
Data/restraints/parameters	1086/0/16			
Lattice parameters (Å)				
a	4.183 27(2)			
c	9.872 78(7)			
Fractional coordinates				
	x	y	z	U(iso) (Å^2)
Ca	0.000 00	0.000 00	0.000 00	0.004 89(24)
Ir	0.000 00	0.000 00	0.646 66(15)	0.002 47(2)
Si(1)	0.000 00	0.000 00	0.409 75(29)	0.004 51(35)
Si(2)	0.000 00	0.500 00	0.258 86(18)	0.004 51(35)
Interatomic distances (Å)				
Ir–Si(1)	2.3396(1)			
Ir–Si(2)	2.3674(1)			
Si(1)–Si(2)	2.5669(1)			
Ca–Si(1)	3.0897(1)			
Ca–Si(2)	3.1687(1)			
Ca–Ir	3.2931(1)			

respectively. The results of the refinement at 100 K are reported in Table II.

III. SUPERCONDUCTING PROPERTIES

A. Dc susceptibility and resistivity

Using polycrystalline samples, dc susceptibility measurements were performed with a commercial Superconducting Quantum Interference Device (SQUID) magnetometer (Quantum Design, MPMS-XL) down to 1.8 K, and resistivity measurements were performed with a commercial instrument (Quantum Design, PPMS) with a ^{3}He refrigeration insert down to 0.35 K using a conventional four-probe technique. Resistivity in zero field up to 300 K for each compound is exhibited in Figs. 4(a) and 4(b). The temperature dependence of the resistivity indicates typical metallic behavior with residual resistivity ratios (RRR, ρ_{300K}/ρ_{5K}) of ∼4 for $CaIrSi_3$ and ∼1.6 for $CaPtSi_3$. The low-temperature resistivity and the

TABLE II. Lattice parameters, fractional atomic coordinates, and interatomic distances for $CaPtSi_3$ at 100 K. U(iso) is the isotropic thermal displacement parameter.

Refinement				
Space group	Tetragonal, $I4mm$ (No. 107)			
Z/calculated density	2/6.133 Mg/m^3			
Absorption coefficient	5.683 mm^{-1}			
Data/restraints/parameters	149/0/5			
Lattice parameters (Å)				
a	4.198 80(10)			
c	9.8111(4)			
Fractional coordinates				
	x	y	z	U(iso) (Å^2)
Ca	0.000 00	0.000 00	0.000 00	0.0036(10)
Pt	0.000 00	0.000 00	0.6429(7)	0.0036(10)
Si(1)	0.000 00	0.000 00	0.3955(12)	0.0036(10)
Si(2)	0.000 00	0.500 00	0.2577(8)	0.0036(10)
Interatomic distances (Å)				
Pt–Si(1)	2.427(14)			
Pt–Si(2)	2.383(5)			
Si(1)–Si(2)	2.497(8)			
Ca–Si(1)	3.141(4)			
Ca–Si(2)	3.172(6)			
Ca–Pt	3.283(3)			

京都大学 KYOTO UNIVERSITY
A Self-archived copy in
Kyoto University Research Information Repository
https://repository.kulib.kyoto-u.ac.jp
京都大学学術情報リポジトリ KURENAI 紅 Kyoto University Research Information Repository

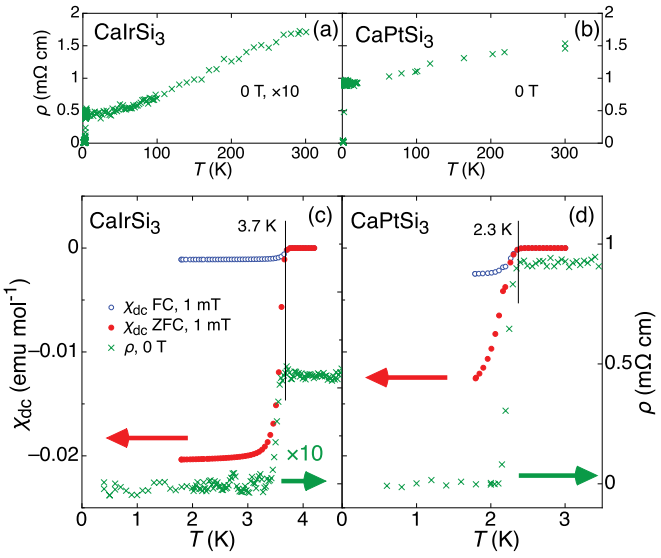

FIG. 4. (Color online) Temperature dependence of the resistivity ρ for (a) $CaIrSi_3$ and (b) $CaPtSi_3$ up to 300 K and low-temperature dc susceptibility χ_{dc} and resistivity for (c) $CaIrSi_3$ and (d) $CaPtSi_3$. Both zero-field-cooled (ZFC) and field-cooled (FC) dc susceptibility under 1 mT are displayed. The onset temperatures of the superconducting transition are approximately 3.7 K for $CaIrSi_3$ and 2.3 K for $CaPtSi_3$ in both measurements. Strong diamagnetism indicates that the majority of each sample was superconducting.

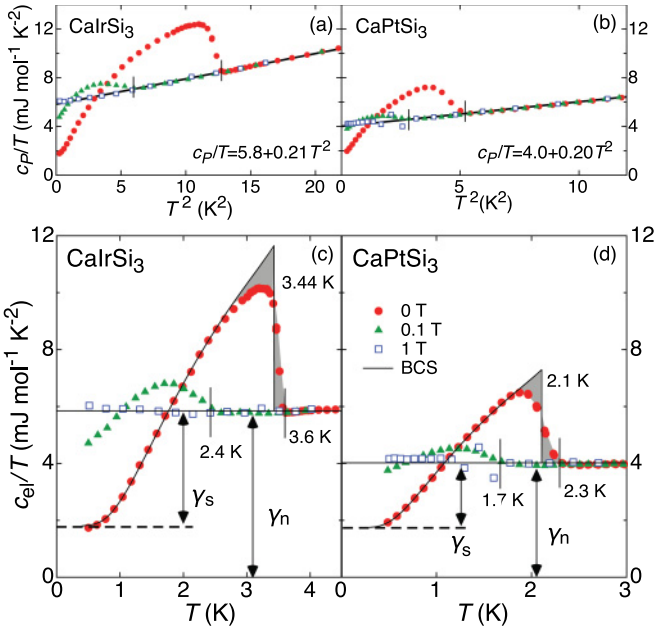

FIG. 5. (Color online) Temperature dependence of total specific heat c_P for (a) $CaIrSi_3$ and (b) $CaPtSi_3$, and electronic specific heat c_{el} for (c) $CaIrSi_3$ and (d) $CaPtSi_3$. T_c onsets in 0 T are 3.6 K for $CaIrSi_3$ and 2.3 K for $CaPtSi_3$, and in 0.1 T are 2.5 K for $CaIrSi_3$ and 1.7 K for $CaPtSi_3$. Solid lines are BCS fits. The shaded regions have the same area on either side of the specific heat jump, corresponding to entropy conservation. The T_c values from this procedure match with those from the BCS fits.

dc susceptibility in 1 mT for each compound, presented in Figs. 4(c) and 4(d), exhibit clear superconducting transitions at 3.7 K for $CaIrSi_3$ and 2.3 K for $CaPtSi_3$. For $CaIrSi_3$ the transition temperature is approximately 20% higher than that reported in Ref. 20, attributed to improved sample quality.

The volume fractions estimated from zero-field cooled dc susceptibility data were ~170% for $CaIrSi_3$ and ~100% for $CaPtSi_3$, assuming the samples to be single phase. These large volume fractions are attributed to neglecting demagnetizing effects, but suggest that a majority of each sample was superconducting. The large difference between field-cooled and zero-field-cooled data is likely due to the presence of melt inclusions that can trap magnetic flux. The RRRs and volume fractions indicate that $CaIrSi_3$ was higher quality than $CaPtSi_3$, consistent with the XRD result.

B. Specific heat

Specific heat measurements were performed down to 0.35 K using a relaxation-time-method calorimeter (Quantum Design, PPMS) on a ^{3}He refrigeration insert. The total specific heat for each compound is presented in Figs. 5(a) and 5(b), and the electronic specific heat in Figs. 5(c) and 5(d). These were calculated assuming the molar weight of the target phases. Superconductivity in both compounds was suppressed by a magnetic field of 1 T. The normal-state specific heat was found to be invariant under external magnetic fields, so the normal-state electronic specific heat coefficients γ_n and the lattice specific heat coefficients β were deduced from the data in 1 T by a least-squares fit of the total specific heat c_P to $\gamma_n T + \beta T^3$. This results in $\gamma_{n,Ir} = 5.8$ mJ/mol K^2 and $\beta_{Ir} = 0.21$ mJ/mol K^4 for $CaIrSi_3$, and $\gamma_{n,Pt} = 4.0$ mJ/mol K^2 and $\beta_{Pt} = 0.20$ mJ/mol K^4 for $CaPtSi_3$. The Debye temperature Θ_D of each compound is estimated from $\beta = (12/5)\pi^4 N_{f.u.} N_A k_B / \Theta_D^3$ as 360 K for $CaIrSi_3$ and 370 K for $CaPtSi_3$, comparable to those found in ordinary metals. Here $N_{f.u.} = 5$ is the number of atoms per formula unit, N_A is Avogadro's number, and k_B is Boltzmann's constant. From the specific heat onsets, we define the transition temperatures $T_c = 3.6$ K for $CaIrSi_3$ and 2.3 K for $CaPtSi_3$ in zero field, consistent with those from dc susceptibility and resistivity. The specific heat jumps indicate the superconductivity to be bulk in nature.

As presented in Figs. 5(c) and 5(d), the electronic specific heat coefficient γ converges to a finite value at low temperatures even in zero field. This indicates that normal-state conduction electrons that do not participate in the superconductivity persist at the Fermi level down to 0 K. However, it cannot be distinguished whether these electrons are contained in $CaIrSi_3$ ($CaPtSi_3$) or in impurity phases.

A fit of c_{el} to a polynomial approximation to the conventional weak-coupling BCS curve tabulated numerically in Ref. 21 is also displayed in Figs. 5(c) and 5(d). The only two free parameters in this procedure are T_c and the superconducting contribution to the electronic specific heat coefficient γ_s. The data are fit up to a T/T_c of just over 70%, and agree well with the BCS curve in this region. The fits result in T_c values of 3.44 K for $CaIrSi_3$ and 2.1 K for $CaPtSi_3$, and γ_s coefficients of 4.0 mJ/mol K^2 for $CaIrSi_3$ and 2.1 mJ/mol K^2 for $CaPtSi_3$. Entropy conservation at the specific heat jump of each compound gives the same T_c [see Figs. 5(c) and 5(d)]. These values of T_c correspond to an average of the T_c distribution in each sample. The superconducting fraction of each sample

京都大学 KYOTO UNIVERSITY
A Self-archived copy in
Kyoto University Research Information Repository
https://repository.kulib.kyoto-u.ac.jp
京都大学学術情報リポジトリ KURENAI 紅 Kyoto University Research Information Repository

is estimated from γ_s/γ_n to be ~70% in $CaIrSi_3$ and ~55% in $CaPtSi_3$, consistent with earlier indications that the $CaPtSi_3$ sample contained a greater proportion of impurity phase. The thermodynamic critical field $\mu_0 H_c(0)$ is estimated using $\mu_0 H_c^2(0)/2 = -\gamma_s T_c^2/2 + \int_0^{T_c} c_{el,s}(T)dT$, where $c_{el,s}(T)$ is the electronic specific heat in the superconducting phase, to be 0.023 T for $CaIrSi_3$ and 0.0094 T for $CaPtSi_3$.

C. Magnetic phase diagram

Measurements of ac susceptibility in various magnetic fields were performed by a mutual-inductance method (1 μT, 3011 Hz) down to 0.3 K using a commercial ^{3}He refrigerator (Oxford Instruments, Heliox) equipped with a superconducting magnet. These and the resistivity results are presented in Fig. 6. The ac susceptibility measurements were performed on both warming and cooling with no hysteresis; thus, only the warming results are displayed. Under magnetic fields, ac susceptibility onsets were observed up to 0.27 T for $CaIrSi_3$ and 0.15 T for $CaPtSi_3$, and resistivity onsets up to 0.6 T for both compounds: several times larger than the thermodynamic critical fields. The large critical fields and nonhysteretic transition temperatures clearly indicate that these compounds are type-II superconductors.

The H–T phase diagrams of $CaIrSi_3$ and $CaPtSi_3$ deduced from the ac susceptibility χ'_{ac} onset, resistivity ρ onset, and specific heat c_P onset are summarized in Fig. 7. The T_c onsets were defined as 5% of full, zero-field diamagnetism in χ'_{ac}, a 5% decrease in ρ, and the onset in c_P. We note that for $CaPtSi_3$ the transition broadens substantially under magnetic fields. This behavior is correlated with the phase purity of the sample as evidenced by impurity peaks in XRD and the larger residual contribution in the specific heat. Each curve is remarkably linear and is slightly concave upward in low magnetic fields. In neither system do the curves deduced from the χ'_{ac} and ρ onsets coincide, and the discrepancy between them is more prominent for $CaPtSi_3$ than for $CaIrSi_3$.

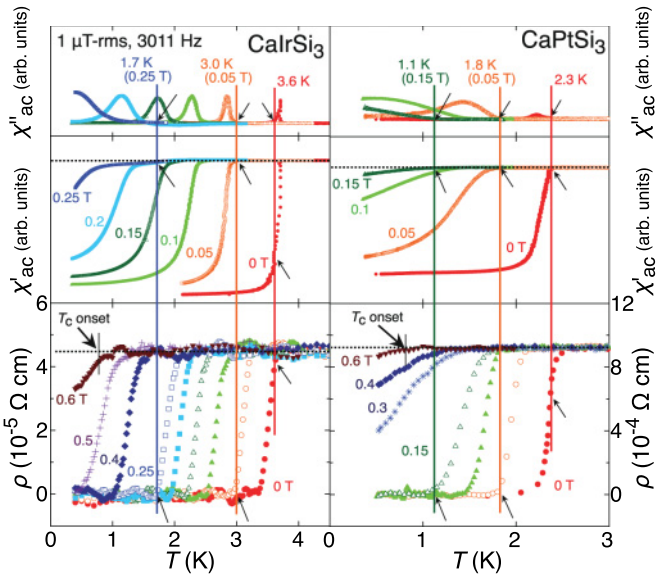

FIG. 6. (Color online) Temperature dependence of ac susceptibility (the imaginary part χ''_{ac} and the real part χ'_{ac}) and resistivity ρ of $CaIrSi_3$ and $CaPtSi_3$ in selected magnetic fields. The zero resistivity temperature matches or exceeds the ac susceptibility onset in magnetic fields. The diamagnetic shielding in χ_{ac} is fully suppressed below 0.3 T for $CaIrSi_3$ and 0.2 T for $CaPtSi_3$, whereas ρ onsets were observed up to 0.6 T.

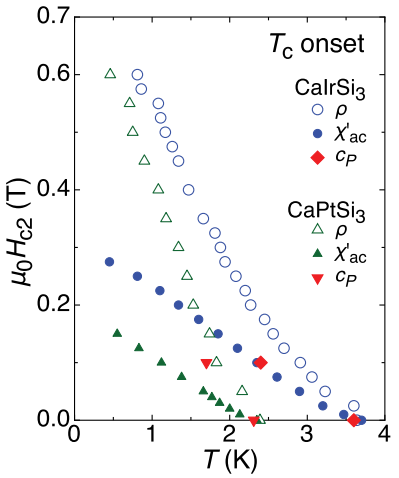

FIG. 7. (Color online) H–T phase diagram of $CaIrSi_3$ and $CaPtSi_3$. Points represent the onset temperatures in χ'_{ac}, ρ, and c_P, as defined in the text. For both compounds the H–T phase lines as extracted from ρ and χ'_{ac} differ. Possible reasons for this difference are discussed in Sec. IV.

Since the H–T curve of $CaIrSi_3$ based on χ'_{ac} onset begins to saturate at high fields, $\mu_0 H_{c2}(0)$ is estimated from the points at 0.3 K as a lower limit and the linear extrapolation to zero temperature as an upper limit: 0.27–0.32 T. Similarly for $CaPtSi_3$ it is estimated as 0.15–0.20 T. Approximate Ginzburg-Landau parameters κ_{GL}, superconducting coherence lengths $\xi(0)$, and penetration depths $\lambda(0)$ are estimated from the $\mu_0 H_{c2}$ lower limits with the relations $\mu_0 H_{c2}(0) = \sqrt{2}\kappa_{GL}\mu_0 H_c(0)$, $\mu_0 H_{c2}(0) = \Phi_0/2\pi\xi^2(0)$, and $\kappa_{GL} = \lambda(0)/\xi(0)$, respectively. These results should be treated with caution since they come from multiphase, polycrystalline samples of anisotropic materials, but they provide an essential starting point. The results are summarized in Table III with the other physical properties determined in this study.

TABLE III. Physical properties of polycrystalline $CaIrSi_3$ and $CaPtSi_3$. Superconducting parameters κ_{GL}, $\xi(0)$, and $\lambda(0)$ are based on the lower limits of $\mu_0 H_{c2}(0)$ determined from χ'_{ac} onset. Note that these values could be affected by sample quality, and in some cases should be anisotropic.

	$CaIrSi_3$	$CaPtSi_3$
T_c	3.6 K	2.3 K
$\mu_0 H_{c2}(0)$ (χ'_{ac} onset)	0.27 T	0.15 T
$\mu_0 H_c(0)$	0.023 T	0.0094 T
κ_{GL}	8.3	11
$\xi(0)$	34 nm	47 nm
$\lambda(0)$	280 nm	520 nm
γ_n	5.8 mJ/mol K^2	4.0 mJ/mol K^2
γ_s	4.0 mJ/mol K^2	2.1 mJ/mol K^2
Θ_D	360 K	370 K

京都大学 KYOTO UNIVERSITY
A Self-archived copy in
Kyoto University Research Information Repository
https://repository.kulib.kyoto-u.ac.jp
京都大学学術情報リポジトリ KURENAI 紅 Kyoto University Research Information Repository

IV. DISCUSSION AND CONCLUSION

The specific heat results are generally well explained by weak-coupling BCS theory and similar to reports on $BaPtSi_3$.[14] While the agreement with the BCS curve suggests that these superconductors are fully gapped, the specific heat of $CaIrSi_3$ falls below this curve just above $0.7T_c$. Although the superconducting transition is broad, this is well outside the transition width. This deviation is suggestive of a departure from a pure s-wave gap structure, as in a multiband or anisotropic-gap scenario, the alternative being an unusual distribution of T_c with a significant tail to low temperatures. The apparent full gap strongly suggests that the superconducting pairing is dominantly or exclusively singlet; a triplet component could introduce gap anisotropy.

The experimental values of $\mu_0 H_{c2}(T)$ are much smaller than the Pauli-limiting fields $\mu_0 H_P(0)$ of $1.84T_c$ expected in weak-coupling s-wave BCS theory, ~6.5 T for $CaIrSi_3$ and ~4 T for $CaPtSi_3$. Barring large corrections to $\mu_0 H_P$, the dominant pair-breaking effect in $CaIrSi_3$ and $CaPtSi_3$ would be orbital depairing. This represents a significant difference from the Ce-containing isostructural superconductors $CeRhSi_3$, $CeIrSi_3$, and $CeCoGe_3$, in which heavy-fermion masses strongly suppress orbital depairing to reveal that Pauli-limiting behavior does not set in where expected for a singlet condensate. Pauli pair breaking is strongly suppressed by the presence of a triplet component or a van Vleck–like susceptibility specific to noncentrosymmetric systems.[4,16,17,22] Unless orbital depairing is also suppressed, however, an extremely high $\mu_0 H_{c2}(0)$ that violates conventional expectations for the Pauli limit, commonly used as a key signature of novel noncentrosymmetric physics, will not be exhibited. This is the case in $CaIrSi_3$ and $CaPtSi_3$, whose small γ values indicate light carrier masses and in which orbital depairing is not suppressed.

In both samples, the $\mu_0 H_{c2}(T)$ obtained from the ac susceptibility and resistivity onsets differ substantially. This discrepancy far exceeds the factor of 1.695 associated with $\mu_0 H_{c3}$ surface superconductivity and thin limit physics, so other effects must be involved. One possible scenario is that anisotropic superconducting parameters, expected given the tetragonal crystal structure, lead to an upper critical field with a strong, narrow peak for one field direction, producing very low volume fractions of robust superconductivity. Another possibility is pressure enhancement of the superconductivity at grain boundaries due to thermal expansion, leading to very thin superconducting surface layers offering a pathway for conductivity but with negligible volume fraction. Finally, the samples could contain networks of more-defected material with almost no volume fraction, in which the mean free path ℓ is shorter than the intrinsic ξ_0. In such a region, the effective coherence length $\xi = (1/\xi_0 + 1/\ell)^{-1}$ is limited by ℓ, increasing $\mu_0 H_{c2} \sim 1/\xi^2$. This would also help to explain a discrepancy with our earlier image furnace-grown $CaIrSi_3$ samples,[20] which have a significantly lower T_c and higher $\mu_0 H_{c2}(0)$. If ξ in the majority of the samples in the present study is dominated by the change in ξ_0, which decreases with decreasing T_c, the broadening of the transition in χ_{ac} can also be coherently explained. The data currently available do not permit determining which of these effects contribute or are dominant. Settling these issues will require single-crystalline samples—anisotropy in the superconducting parameters would be readily apparent when varying the field angle, pressure effects could be studied, and magnetic and nonmagnetic impurities could be doped in to test their effect controllably.

An upward curvature in low fields and striking linearity of $\mu_0 H_{c2}(T)$ are observed in both compounds. Such behavior is quite uncommon, but has been observed in multiband superconductors, for example, MgB_2.[23] With the full crystal structure determined in $CaIrSi_3$ and $CaPtSi_3$, band-structure calculations may now be performed to predict the shape of the Fermi surface and whether multiband physics is likely to play a role. This is noteworthy since, to the authors' knowledge, atomic positions have never been published for the Ce analog, although they have been for $LaIrSi_3$ and $LaRhSi_3$,[24] nonsuperconducting $CePtSi_3$,[25] and $BaPtSi_3$.[14]

One somewhat surprising result is that $CaIrSi_3$, $CaPtSi_3$, and previously published $BaPtSi_3$[14] all behave in a very similar fashion. The only clear qualitative differences are in the transition widths and the magnitude of the difference between the T_c onsets. Because the spin-orbit coupling strength is expected to increase strongly with atomic number, all three materials are expected to exhibit strong band splitting. Although the Pt-based materials should have somewhat stronger band splitting, its effect on the physical properties will hinge on details of the band structure. In order to determine whether or not noncentrosymmetric physics is operative in these materials, microscopic techniques such as nuclear magnetic resonance or μSR may prove useful.

In conclusion, we reported the crystallographic and superconducting properties of $CaIrSi_3$ and $CaPtSi_3$. The electronic specific heat coefficients γ are a few mJ/mol K^2 in both $CaIrSi_3$ and $CaPtSi_3$, values not unusual for metals, indicating that the electron correlations are not strong in these compounds. Their specific heat results suggest that these superconductors are fully gapped. The upper critical fields $\mu_0 H_{c2}(0)$ are less than a Tesla and consistent with a conventional orbital depairing mechanism. This and the small γ values constitute a significant departure from the heavy-fermion Ce-based materials. Because several results have multiple possible interpretations and the role of anisotropy is unclear, single-crystalline samples will be required. Our results on the promising $5d$-electron analogs of known Ce-based materials lay the groundwork for studies of the importance of heavy electrons in noncentrosymmetric superconductors.

ACKNOWLEDGMENTS

We thank S. Yonezawa, H. Takatsu, S. Kittaka, Y. Tada, S. Fujimoto, C. Michioka, and K. Yoshimura for fruitful discussions and useful advice. The synchrotron radiation experiments performed at BL02B1 and BL02B2 at SPring-8 were supported by the Japan Synchrotron Radiation Research Institute (JASRI) (Proposal No. 2009A,B0083,0084). This work is supported by a Grant-in-Aid from the Global COE program "The Next Generation of Physics, Spun from Universality and Emergence" from the Ministry of Education, Culture, Sports, Science, and Technology (MEXT) of Japan, and by the "Topological Quantum Phenomena" Grant-in Aid for Scientific Research on Innovative Areas from MEXT of

京都大学 KYOTO UNIVERSITY
A Self-archived copy in
Kyoto University Research Information Repository
https://repository.kulib.kyoto-u.ac.jp
京都大学学術情報リポジトリ KURENAI 紅 Kyoto University Research Information Repository

TABLE IV. Crystal data and structure refinement parameters of $CaIr_3Si_7$ at 100 K. The equivalent isotropic displacement parameter $U(\text{eq})$ is defined as one third of the trace of the orthogonalized U_{ij} tensor.

Refinement				
Space group	Rhombohedral, $R\bar{3}c$ (No. 167)			
Z/calculated density	6/8.143 Mg/m^3			
Absorption coefficient	33.609 mm^{-1}			
Data/restraints/parameters	1816/0/20			
Extinction coefficient	0.000 16(15)			
Lattice parameters (Å)				
a	7.5782(3)			
c	20.0091(2)			
Fractional coordinates				
	x	y	z	$U(\text{eq})$ (Å^2)
Ir	0.346 499(17)	0.013 165(17)	0.083 33	0.002 05(3)
Ca	0.000 00	0.000 00	0.000 00	0.003 08(10)
Si(1)	0.462 34(11)	0.142 40(11)	−0.029 62(4)	0.003 38(8)
Si(2)	0.666 67	0.333 33	0.083 33	0.002 37(17)
Interatomic distances (Å)				
Ir–Si(2)	2.426 30(13)			
Ir–Si(1)	2.4449(7)			
Ir–Si(1)	2.4526(7)			
Ir–Si(1)	2.5201(7)			
Ir–Ca	3.0697(1)			
Ca–Si(1)	3.1257(7)			
Si(1)–Si(1)	2.5985(13)			
Si(1)–Si(2)	2.7127(7)			
Si(1)–Si(1)	2.7365(15)			
Si(1)–Si(1)	2.7605(15)			

Japan. G.E., M.K., and D.C.P. are supported by the Japan Society for the Promotion of Science (JSPS).

APPENDIX: THE NEW MATERIAL $CaIr_3Si_7$

While optimizing the preparation technique for $CaIrSi_3$, the previously unreported ternary phase $CaIr_3Si_7$ was discovered, and subsequently reproduced by solid-state reaction of Ca:Ir:Si = 1:1:3 under vacuum in a sealed quartz tube (1100°C, 24 hours). This compound crystallizes in the rhombohedral space group $R\bar{3}c$ (No. 167), isotypic to $ScRh_3Si_7$ and $ScIr_3Si_7$,[26] and possesses an inversion center. It does not exhibit superconductivity above 1.8 K. We note that thorough investigation of the synthesis of $CaPtSi_3$ by a flux method by Takeuchi *et al.* resulted in synthesizing a new centrosymmetric superconductor, $Ca_2Pt_3Si_5$.[27]

A single-crystalline grain of $CaIr_3Si_7$, prepared by melting a mixture of stoichiometry Ca:Ir:Si = 1:1:3 in an image furnace, was separated from excess melt phases using dilute hydrochloric acid. This grain was then characterized at room temperature by single-crystal x-ray diffraction at SPring-8 beam line BL02B1[28] using a large cylindrical image plate detector. A wavelength of 0.351 00 Å was used, and data were collected over the index range $0 \leqslant h \leqslant 16$, $0 \leqslant k \leqslant 16$, and $0 \leqslant l \leqslant 49$, and over a range in θ of 1.83° to 26.02°. A total of 1816 reflections were collected, all of which were unique and 1697 of which had intensity $>2\sigma(I)$. The structure was solved and refined using SHELXS97 and SHELXL97, respectively;[29] results are summarized in Table IV. Refinement was by a full-matrix least-squares minimization of F^2. The final reliability factors R_1 and wR_2 were 2.04% and 7.11%, respectively, on peaks with intensity greater than $2\sigma(I)$, and 2.70% and 7.93%, respectively, on all data.

Since this crystal structure contains a large number of atoms per unit cell in a nontrivial arrangement, it must be broken into

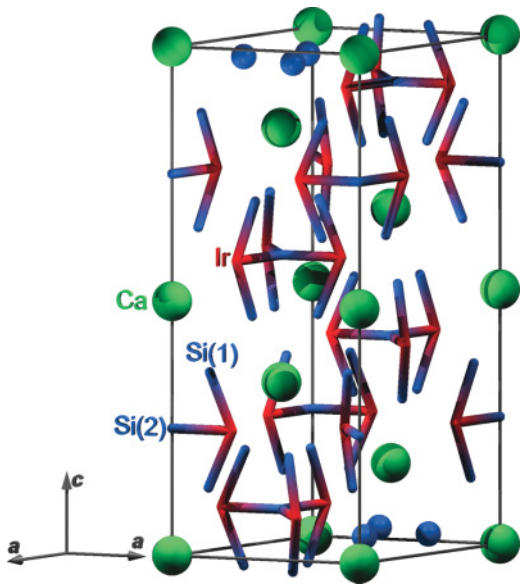

FIG. 8. (Color online) Crystal structure of $CaIr_3Si_7$ as determined by single-crystal x-ray diffraction.

京都大学 KYOTO UNIVERSITY
A Self-archived copy in
Kyoto University Research Information Repository
https://repository.kulib.kyoto-u.ac.jp
京都大学学術情報リポジトリ KURENAI 紅 Kyoto University Research Information Repository

subunits to be described. As $ScRh_3Si_7$, it was portrayed as an array of Sc(Ca)-centered Rh(Ir) octahedra and Si double tetrahedra in which the shared apex was the Si(2) site.[26] However, since the shortest bonds in the material are those between Rh(Ir) and Si, it may be more realistic to visualize the structure in terms of slightly twisted Si-centered Ir_3Si_7 barrels and isolated Ca atoms. A crystal structure based on this scheme is presented in Fig. 8.

*geguchi@scphys.kyoto-u.ac.jp

[1]E. Bauer, G. Hilscher, H. Michor, C. Paul, E. W. Scheidt, A. Gribanov, Y. Seropegin, H. Noël, M. Sigrist, and P. Rogl, Phys. Rev. Lett. **92**, 027003 (2004).
[2]V. M. Edelstein, Phys. Rev. Lett. **75**, 2004 (1995).
[3]P. A. Frigeri, D. F. Agterberg, A. Koga, and M. Sigrist, Phys. Rev. Lett. **92**, 097001 (2004).
[4]S. Fujimoto, J. Phys. Soc. Jpn. **76**, 051008 (2007).
[5]Y. Yanase and M. Sigrist, J. Phys. Soc. Jpn. **76**, 124709 (2007).
[6]T. Akazawa, H. Hidaka, H. Kotegawa, T. C. Kobayashi, T. Fujiwara, E. Yamamoto, Y. Haga, R. Settai, and Y. Ōnuki, J. Phys. Soc. Jpn. **73**, 3129 (2004).
[7]N. Kimura, K. Ito, K. Saitoh, Y. Umeda, H. Aoki, and T. Terashima, Phys. Rev. Lett. **95**, 247004 (2005).
[8]T. Shibayama, M. Nohara, H. A. Katori, Y. Okamoto, Z. Hiroi, and H. Takagi, J. Phys. Soc. Jpn. **76**, 073708 (2007).
[9]Z.-A. Ren, J. Kato, T. Muranaka, J. Akimitsu, M. Kriener, and Y. Maeno, J. Phys. Soc. Jpn. **76**, 103710 (2007).
[10]H. Q. Yuan, D. F. Agterberg, N. Hayashi, P. Badica, D. Vandervelde, K. Togano, M. Sigrist, and M. B. Salamon, Phys. Rev. Lett. **97**, 017006 (2006).
[11]M. Nishiyama, Y. Inada, and G.-q. Zheng, Phys. Rev. Lett. **98**, 047002 (2007).
[12]A. D. Hillier, J. Quintanilla, and R. Cywinski, Phys. Rev. Lett. **102**, 117007 (2009).
[13]S. Oikawa, M. Nohara, and H. Takagi, Presented at the 63rd JPS Fall meeting, 23pQC (2008).
[14]E. Bauer, R. T. Khan, H. Michor, E. Royanian, A. Grytsiv, N. Melnychenko-Koblyuk, P. Rogl, D. Reith, R. Podloucky, E.-W. Scheidt, W. Wolf, and M. Marsman, Phys. Rev. B **80**, 064504 (2009).
[15]N. Kimura, Y. Muro, and H. Aoki, J. Phys. Soc. Jpn. **76**, 051010 (2007).
[16]I. Sugitani, Y. Okuda, H. Shishido, T. Yamada, A. Thamizhavel, E. Yamamoto, T. D. Matsuda, Y. Haga, T. Takeuchi, R. Settai, and Y. Ōnuki, J. Phys. Soc. Jpn. **75**, 043703 (2006).
[17]R. Settai, I. Sugitani, Y. Ōnuki, T. D. Matsuda, Y. Haga, and H. Harada, Int. J. Mod. Phys. B **21**, 3238 (2007).
[18]E. Nishibori, M. Takata, K. Kato, M. Sakata, Y. Kubota, S. Aoyagi, Y. Kuroiwa, M. Yamakata, and N. Ikeda, Nucl. Instrum. Methods Phys. Res. A **467-468**, 1045 (2001).
[19]E. Nishibori, E. Sunaoshi, A. Yoshida, S. Aoyagi, K. Kato, M. Takata, and M. Sakata, Acta Cryst. A **63**, 43 (2007).
[20]G. Eguchi, D. Peets, M. Kriener, S. Maki, E. Nishibori, H. Sawa, and Y. Maeno, Physica C **470**, S762 (2010).
[21]B. Mühlschlegel, Z. Phys. **155**, 313 (1959).
[22]N. Kimura, K. Ito, H. Aoki, S. Uji, and T. Terashima, Phys. Rev. Lett. **98**, 197001 (2007).
[23]J. Karpinski, M. Angst, J. Jun, S. M. Kazakov, R. Puzniak, A. Wisniewski, J. Roos, H. Keller, A. Perucchi, L. Degiorgi, M. R. Eskildsen, P. Bordet, L. Vinnikov, and A. Mironov, Supercond. Sci. Technol. **16**, 221 (2003).
[24]P. Lejay, I. Higashi, B. Chevalier, J. Etourneau, and P. Hagenmuller, Mater. Res. Bull. **19**, 115 (1984).
[25]T. Kawai, Y. Okuda, H. Shishido, A. Thamizhavel, T. D. Matsuda, Y. Haga, M. Nakashima, T. Takeuchi, M. Hedo, Y. Uwatoko, R. Settai, and Y. Ōnuki, J. Phys. Soc. Jpn. **76**, 014710 (2007).
[26]B. Chabot, N. Engel, and E. Parthé, Acta Cryst. B **37**, 671 (1981).
[27]T. Takeuchi, H. Muranaka, R. Settai, T. D. Matsuda, E. Yamamoto, Y. Haga, and Y. Ōnuki, J. Phys. Soc. Jpn. **78**, 085001 (2009).
[28]Y. Noda, K. ichi Ohshima, H. Toraya, K. Tanaka, H. Terauchi, H. Maeta, and H. Konishi, J. Synchrotron Rad. **5**, 485 (1998).
[29]G. M. Sheldrick, Acta Cryst. A **64**, 112 (2008).